



Cite this: *Phys. Chem. Chem. Phys.*,
2015, 17, 19874

Configuration coordinate energy level diagrams of intervalence and metal-to-metal charge transfer states of dopant pairs in solids

Zoila Barandiarán,^{ab} Andries Meijerink^c and Luis Seijo^{*ab}

Configuration coordinate diagrams, which are normally used in a qualitative manner for the energy levels of active centers in phosphors, are quantitatively obtained here for intervalence charge transfer (IVCT) states of mixed valence pairs and metal-to-metal charge transfer (MMCT) states of heteronuclear pairs, in solid hosts. The procedure relies on vibrational frequencies and excitation energies of single-ion active centers, and on differences between ion–ligand distances of the donor and the acceptor, which are attainable empirically or through *ab initio* calculations. The configuration coordinate diagrams of the Yb²⁺/Yb³⁺ mixed-valence pair in Yb-doped YAG and the Ce³⁺/Yb³⁺ heteronuclear pair in Ce,Yb-codoped YAG, are obtained and described. They are drawn from empirical data of the single-ions and their usefulness is discussed. The first diagram suggests that IVCT states of Yb²⁺/Yb³⁺ pairs may play an important role in the quenching of the Yb³⁺ emission and it provides the details of the quenching mechanism. The second diagram supports the interpretation recently given for the energy transfer from Ce³⁺ to Yb³⁺ in Ce,Yb-codoped YAG via a MMCT Ce⁴⁺–Yb²⁺ state and it provides the details. The analyses of the two diagrams suggest the formation of Yb²⁺/Yb³⁺ pairs after the Ce³⁺-to-Yb³⁺ MMCT, which is responsible for the temperature quenching of the Yb³⁺ emission excited via Ce³⁺ (4f → 5d) absorption in Ce,Yb-codoped YAG.

Received 6th May 2015,
Accepted 26th June 2015

DOI: 10.1039/c5cp02625c

www.rsc.org/pccp

1. Introduction

Electron transfer between two metal ions involved in a redox process is an important phenomenon in biology, chemistry, and materials science. It is often known as metal-to-metal charge transfer (MMCT). When the two metal ions differ only in the oxidation state, the conventional name of this process is intervalence charge transfer (IVCT).¹ [The term IVCT is used sometimes for MMCT between non-equivalent metal ions and also for electron transfer processes not involving metals; here we will adopt the conventional meaning and we will call IVCT only to the homonuclear, symmetric MMCT.]

MMCT states are considered to have an important role in energy transfer processes between optically active centers of doped solids and in non-radiative decays which can drastically change the optical behavior of materials.² The blue to near-infrared conversion in Ce³⁺,Yb³⁺-codoped YAG (ref. 3) and the ultraviolet

to greenish-blue or to red conversions in Pr³⁺-doped CaTiO₃ and CaZrO₃ (ref. 4) are respective examples.

IVCT absorption, which has been found in a large number of mixed-valence molecular compounds,^{5,6} has also been reported in lanthanide activated phosphors like Ce³⁺-doped LaPO₄ (ref. 7), and lanthanide mixed-valence solids like Na₅Eu₇Cl₂₂ (ref. 8). And IVCT luminescence has recently been reported to exist as well, and to be responsible for the anomalous emission of Ce³⁺ in elpasolites⁹ and Yb²⁺ in fluorites.¹⁰ In fact, the IVCT states of mixed-valence pairs in doped solids have a high potential for changing the absorption, emission, and non-radiative decays of the materials when the pairs are formed, because these states are intercalated between the regular states of single-ion active centers.^{9,10} Hence a detailed knowledge of the IVCT states in materials where such mixed-valence pairs are likely to form is important. Among others, this could be the case of solids activated by Ce³⁺, Pr³⁺, Eu²⁺, or Yb²⁺ lanthanide dopants, in which preventing the coexistence of several valence states is difficult.^{11,12}

It is common to address the participation of MMCT and IVCT states in energy transfer, non-radiative decay, and radiative processes with the help of schematic configuration coordinate energy level diagrams^{2–4,7} (cf. Fig. 4 in ref. 7, for instance). Here, we present an alternative to make quantitative IVCT and MMCT configuration coordinate diagrams using structural and energetic

^a Departamento de Química, Universidad Autónoma de Madrid, 28049 Madrid, Spain. E-mail: luis.seijo@uam.es

^b Instituto Universitario de Ciencia de Materiales Nicolás Cabrera, Universidad Autónoma de Madrid, 28049 Madrid, Spain

^c Condensed Matter and Interfaces, Debye Institute for Nanomaterials Science, Utrecht University, Princetonplein 5, 3584 CC Utrecht, The Netherlands

data of the single-ion active centers, which are attainable empirically or through *ab initio* calculations. We discuss their meaning and use them as interpretative tools for the issues mentioned above.

As bases for the elaboration of the IVCT and MMCT configuration coordinate diagrams, we take the vibronic model for the IVCT absorption of the two-state problem of a mixed-valence pair of Piepho *et al.*¹³ and its extension to excited states, which was used to analyze state-of-the-art *ab initio* calculations of the diabatic potential energy surfaces of Ce³⁺/Ce⁴⁺ and Yb²⁺/Yb³⁺ pairs of dopant ions in solids.^{9,10} The latter revealed that even though adiabatic potential energy surfaces calculated by a full consideration of electronic couplings between electronic states of donor and acceptor centres are necessary for IVCT absorption and emission intensities and non-radiative decay rates, a great deal of quantitative spectroscopic information on the pairs can be attained at the diabatic level, *i.e.* without explicit consideration of donor–acceptor electronic couplings. Hence, we focus here on the diabatic approximation to configuration coordinate diagrams.

We discuss the definition of the configuration coordinate of a single-ion active center and its corresponding energy level diagram in Section II. This serves as a basis for the definition of the IVCT configuration coordinate of a mixed-valence pair in Section III, where the corresponding energy level diagram is discussed. The same is done for the MMCT states of a heteronuclear metallic pair in Section IV. Detailed discussions of IVCT and MMCT sample cases are given: the Yb²⁺/Yb³⁺ mixed-valence pair in YAG, Section III.B, and the Ce³⁺/Yb³⁺ heteronuclear pair in YAG, Section IV.B.

II. Configuration coordinate of a single ion active center

Let us briefly discuss on the configuration coordinate of a single ion active center and its corresponding configuration coordinate diagram. This diagram is a very useful simplified representation of the variation in energy of the electronic levels of the active center with the nuclear displacements. In this simplified description, only one vibrational coordinate is used, which is called the configuration coordinate, and the diagram is aimed at providing gross details of the crossings and relative positions of the electronic levels. Fine details, such as Jahn–Teller distortions, demand the use of several vibrational coordinates.

Let us consider the energies of the electronic levels of an optically active center with a single ion in the absence of (Jahn–Teller) vibronic couplings between degenerate states. The potential energy surface of the active center in its ground state can be written as a function of its normal vibrational coordinates as

$$E_0(Q_1, Q_2, \dots) = \frac{1}{2} \sum_{\mu}^{N_{\text{TS}}} k_{\mu 0} Q_{\mu}^2 + \frac{1}{2} \sum_{\nu}^{N_{\text{NTS}}} k_{\nu 0} Q_{\nu}^2 + \dots \quad (1)$$

In this expression, the ground state electronic energy at equilibrium is taken as a reference for the energy scale, and the equilibrium structure is the reference for the vibrational coordinates. In eqn (1), the leading terms are quadratic and diagonal, and, for convenience, we have divided the normal modes into N_{TS} totally symmetric, $\{Q_{\mu}\}$,

and N_{NTS} non-totally symmetric, $\{Q_{\nu}\}$. Then, the energy of an excited electronic state, E_i , can be written as

$$E_i(Q_1, Q_2, \dots) = E_{i,e} + \frac{1}{2} \sum_{\mu}^{N_{\text{TS}}} k_{\mu i} (Q_{\mu} - Q_{\mu i})^2 + \frac{1}{2} \sum_{\nu}^{N_{\text{NTS}}} k_{\nu i} Q_{\nu}^2 + \dots \quad (2)$$

Here, $E_{i,e}$ is the the minimum-to-minimum excitation energy from the ground state (vertical offset), $Q_{\mu i}$ is the vibrational offset of the Q_{μ} totally symmetric normal mode with the ground state (horizontal offset), and it is clear that non-totally symmetric normal modes have null offsets (because symmetry makes all linear Q_{ν} terms of the electronic energy vanish). Eqn (2) implies that non-totally symmetric normal modes only contribute to the electronic energy difference if the respective force constants are different, *e.g.* $k_{\nu 0} \neq k_{\nu i}$. Usually, such contributions are much smaller than those due to vibrational equilibrium offsets. So, the leading term of $E_i - E_0$ is due to the totally symmetric vibrational modes,

$$E_i(Q_1, Q_2, \dots) - E_0(Q_1, Q_2, \dots) = E_{i,e} + \frac{1}{2} \sum_{\mu}^{N_{\text{TS}}} k_{\mu i} (Q_{\mu} - Q_{\mu i})^2 - \frac{1}{2} \sum_{\mu}^{N_{\text{TS}}} k_{\mu 0} Q_{\mu}^2 + \dots \quad (3)$$

In some highly symmetric active centers, like O_h octahedral ML₆ sites and cubic ML₈ sites, only the breathing modes are totally symmetric. In these cases, if the vibration of the first coordination shell is the only relevant vibration, then one single breathing mode contributes in eqn (3),

$$Q_{\text{breath}} = \frac{1}{\sqrt{n}} (\delta_{L_1} + \delta_{L_2} + \dots + \delta_{L_n}), \quad (4)$$

with n being the number of breathing ligands and δ_{L_i} the increment of the M – L_i distance with respect to its value in the reference structure.

In a more general case, it is convenient to define a configuration coordinate. In effect, we can make a rotation (unitary transformation) of the N_{TS} totally symmetric vibrational coordinates into a new set $\{Q_{\mu'}\}$, such that one of the transformed coordinates connects directly the minima of the ground and excited states. Let us call this coordinate Q_{eff} . (We represent in Fig. 1 the original and transformed coordinates in the case of two totally symmetric coordinates Q_1 and Q_2 .) Then, E_i and E_0 will have a horizontal offset in this coordinate Q_{eff} , but their offset in all other vibrational coordinates will be zero. Accordingly, only the Q_{eff} vibrational mode contributes to the leading term of the $E_i - E_0$ energy difference,

$$E_i(Q_1, Q_2, \dots) - E_0(Q_1, Q_2, \dots) = E_{i,e} + \frac{1}{2} k_{\text{eff},i} (Q_{\text{eff}} - Q_{\text{eff},i})^2 - \frac{1}{2} k_{\text{eff},0} Q_{\text{eff}}^2 + \dots \quad (5)$$

Q_{eff} is, then, the configuration coordinate of the single ion active center, because it is the only one with the horizontal

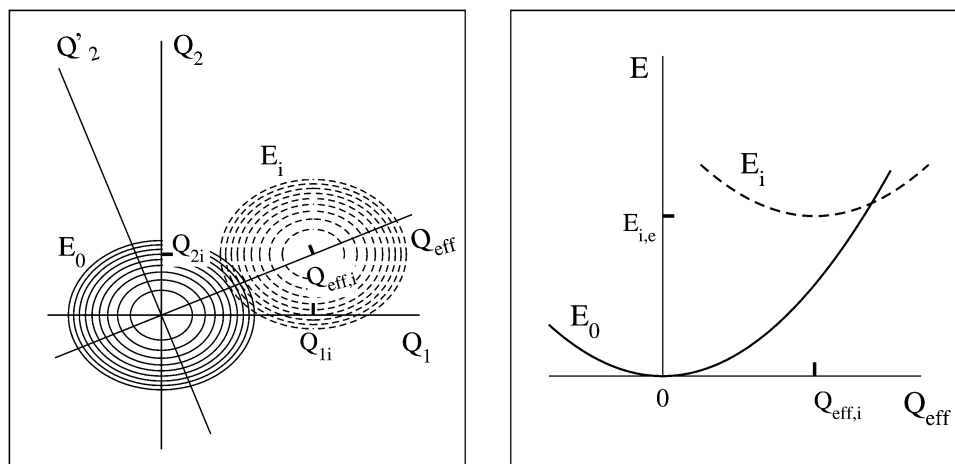


Fig. 1 Left: Definition of the configuration coordinate Q_{eff} of a single ion active center with two totally symmetric normal vibrational modes Q_1 and Q_2 . The ground state E_0 and one excited state E_i potential energy surfaces are shown. Right: Corresponding configuration coordinate energy diagram.

offset and the only one that contributes to the leading term of the electronic energy differences.

[We may remark that this configuration coordinate for the potential energy surfaces of two states (ground and excited) is totally equivalent to the reaction coordinate defined between two minima of the potential energy surface of a chemical reaction (reactants and products). Accordingly, for higher-order approximations to the state energies in eqn (3), the configuration coordinate is not exactly the straight line connecting the minima, but the curve that connects the lowest energy crossing point between the two surfaces with the two minima, with the maximum descendent slope. However, we will assume that the quadratic approximation is valid for our purposes.]

We must bear in mind that, in general, the transformed vibrational coordinates are not normal modes, *i.e.* there are $Q_{eff}Q_{\mu'}$ off-diagonal quadratic terms contributing to the electronic energies. If these terms are negligible, eqn (5) holds and Q_{eff} is a real vibrational coordinate that connects the minima of E_0 and E_i . Also, if all excited states have their minima aligned with E_0 and E_i in the vibrational space, Q_{eff} is uniquely defined for all states. In contrast, if $Q_{eff}Q_{\mu'}$ off-diagonal terms are important or the electronic energy minima of all states are far from being aligned, then, for eqn (5) to hold for all excited states, Q_{eff} must be some sort of not well defined, effective vibrational coordinate. For simplicity, Q_{eff} is often abbreviated as Q . The representation of the energies of the electronic states of the single ion active center along Q is called the configuration coordinate diagram.

III. IVCT configuration coordinate diagram of a mixed valence pair

In this section we describe the configuration coordinate diagram of the intervalence charge transfer (IVCT) states of donor-acceptor dopant pairs in a solid host. We will take an Yb^{2+}/Yb^{3+} mixed valence pair in Yb-doped YAG ($Y_3Al_5O_{12}$) as a working example. We will assume both Yb ions substitute for Y at a D_2 symmetry site with 8-fold oxygen coordination (with long-range

Table 1 Level energies relative to their respective ground states ($E_{i,e}$, in cm^{-1}) and an increase of the average Yb–O and Ce–O distances with respect to their values in the ground states of YAG: Yb^{3+} and YAG: Ce^{3+} , respectively (Δd , in Å)

Level	$E_{i,e}^a$	Δd^e	Level	$E_{i,e}^b$	Δd^e
YAG: Yb^{3+}			YAG: Ce^{3+}		
4f ¹³ levels			4f ¹ levels		
1 $\Gamma_5(^2F_{7/2})$	0	0	1 $\Gamma_5(^2F_{5/2})$	0	0
2 $\Gamma_5(^2F_{7/2})$	611	0.00	2 $\Gamma_5(^2F_{5/2})$	289	0.00
3 $\Gamma_5(^2F_{7/2})$	696	0.00	3 $\Gamma_5(^2F_{5/2})$	770 ^c	0.00
4 $\Gamma_5(^2F_{7/2})$	782	0.00	4 $\Gamma_5(^2F_{7/2})$	2112	0.00
5 $\Gamma_5(^2F_{5/2})$	10 321	0.00	5 $\Gamma_5(^2F_{7/2})$	2342	0.00
6 $\Gamma_5(^2F_{5/2})$	10 620	0.00	6 $\Gamma_5(^2F_{7/2})$	2466	0.00
7 $\Gamma_5(^2F_{5/2})$	10 674	0.00	7 $\Gamma_5(^2F_{7/2})$	3830	0.00
			Lowest 5d ¹ level		
			8 $\Gamma_5(5d)$		
			20 450 ^d		
YAG: Yb^{2+}			YAG: Ce^{4+}		
A	0	0.14	A	0	–0.16

^a Ref. 14. ^b Ref. 15. ^c Ref. 16. ^d Ref. 17. ^e See text.

charge compensation in the case of Yb^{2+}) and we will focus on the 4f^N manifold. Consequently, we are interested in the energy levels resulting from the interplay between the 4f¹⁴ electronic configuration of Yb^{2+} and the 4f¹³ electronic configuration of Yb^{3+} . The 4f¹⁴ closed-shell configuration of Yb^{2+} has a single totally symmetric A state. As is shown in Table 1, the 4f¹³ open-shell configuration of Yb^{3+} has seven Γ_5 Kramer's doublets which are grouped into four $^2F_{7/2}$ related levels spanning about 800 cm^{-1} and three $^2F_{5/2}$ related levels spanning about 500 cm^{-1} and lying at about 10 000 cm^{-1} above.¹⁴

Let us label the two distinguishable Yb dopant atoms of an Yb^{2+}/Yb^{3+} mixed valence pair as Yb_L and Yb_R . Starting with an $Yb_L^{2+}-Yb_R^{3+}$ ionic configuration of the pair, we have seven levels with the same relative energies of the Yb^{3+} levels. Besides these states, we have those that result from electron transfer from Yb^{2+} to Yb^{3+} . Such electron transfer produces an $Yb_L^{3+}-Yb_R^{2+}$ ionic configuration of the pair, which also has seven levels with the same relative energies of the Yb^{3+} levels. These are called the IVCT states (of the original, reference $Yb_L^{2+}-Yb_R^{3+}$ pair; obviously, the two sets of seven states are each others' IVCT states.) Altogether, the 4f^N manifold of an Yb^{2+}/Yb^{3+}

mixed valence pair in YAG is made of 14 energy levels. The energies of the seven levels of the $\text{Yb}_L^{2+}\text{-Yb}_R^{3+}$ ionic configuration vary with the displacements of the oxygen atoms around Yb_L and Yb_R , but their differences are very insensitive to these displacements because of the $5s^25p^6$ shielding of the 4f shells. The same is true for the seven levels of the $\text{Yb}_L^{3+}\text{-Yb}_R^{2+}$ ionic configuration. In contrast, the energy differences between the two sets of levels are very much dependent on the positions of the oxygen atoms because they involve ionization at one site and electron attachment at the complementary site. Here we describe this dependence.

A. IVCT model

In order to facilitate the extension to other mixed valence pairs and to simplify the notation, we will call Yb^{2+} the donor D and Yb^{3+} the acceptor A. More precisely, D and A will not refer to the single Yb ions, but to the defect centers they create in the solid; usually these are atomic moieties containing the Yb ions and their first coordination shells at least. Then the $\text{Yb}_L^{2+}\text{-Yb}_R^{3+}$ ionic configuration of the $\text{Yb}^{2+}/\text{Yb}^{3+}$ mixed valence pair can be called D_LA_R , or simply DA, and the $\text{Yb}_L^{3+}\text{-Yb}_R^{2+}$ ionic configuration A_LD_R , or simply AD.

Let us describe first the energy of the electronic ground state of the $\text{Yb}^{2+}/\text{Yb}^{3+}$ mixed valence pair as a function of two normal modes Q_L and Q_R , which describe vibrations around Yb_L and Yb_R respectively. We will comment later on the excited states. We may think of Q_L and Q_R as the configuration coordinates (Section II) of the Yb_L and Yb_R active centers. In general, they can be any totally symmetric normal vibrational coordinate of the centers.

The adiabatic ground state energy of the $\text{Yb}^{2+}/\text{Yb}^{3+}$ pair at any value of Q_L and Q_R can be seen as a result of the diagonalization of a 2×2 Hermitean matrix whose diagonal elements are the energies of the $\text{Yb}_L^{2+}\text{-Yb}_R^{3+}$ and $\text{Yb}_L^{3+}\text{-Yb}_R^{2+}$ ionic configurations of the pair

(diabatic energies $H_{11} = E_{\text{D}_0\text{A}_0}$ and $H_{22} = E_{\text{A}_0\text{D}_0}$), and with the electronic coupling between the two ionic configurations as the off-diagonal element H_{12} . This diagonalization also gives the adiabatic energy of a second, excited state at each Q_L and Q_R . The consideration of the H_{12} electronic coupling is central to the energy barrier of the thermal electron transfer reaction $\text{Yb}_L^{2+}\text{-Yb}_R^{3+} \rightarrow \text{Yb}_L^{3+}\text{-Yb}_R^{2+}$ and to the radiative and non-radiative transition probabilities. However, it is of minor importance for the energy of the corresponding optical electron transfer, which takes place at a fixed equilibrium structure of $\text{Yb}_L^{2+}\text{-Yb}_R^{3+}$ with a relatively long Yb–Yb distance, and for the values of the vibrational coordinates at which crossings between potential energy surfaces occur.^{9,10} In consequence, we will discuss the diabatic energies of $\text{Yb}_L^{2+}\text{-Yb}_R^{3+}$ and $\text{Yb}_L^{3+}\text{-Yb}_R^{2+}$, which correspond to null electronic coupling between the oxidized and reduced members of the pair.

The diabatic energy of the ground state of the DA ionic configuration, as a function of the positions of the ligands that can be described using the coordinates Q_L and Q_R , can be written as

$$E_{\text{D}_0\text{A}_0}(Q_L, Q_R) = \frac{1}{2}k(Q_L - Q_{\text{D}_0})^2 + \frac{1}{2}k(Q_R - Q_{\text{A}_0})^2, \quad (6)$$

in a quadratic approximation with a common force constant for D and A, $k = \mu\omega^2$, μ being the reduced mass of the vibration and ω the vibrational frequency common to both vibrational coordinates. This equation establishes the minimum of $E_{\text{D}_0\text{A}_0}$ as the reference energy. Q_{D_0} and Q_{A_0} are the values of the vibrational coordinates at the equilibrium structures of D and A respectively. Equivalently, if the donor and acceptor sites are identical, the diabatic energy of the ground state of the AD ionic configuration is

$$E_{\text{A}_0\text{D}_0}(Q_L, Q_R) = \frac{1}{2}k(Q_L - Q_{\text{A}_0})^2 + \frac{1}{2}k(Q_R - Q_{\text{D}_0})^2. \quad (7)$$

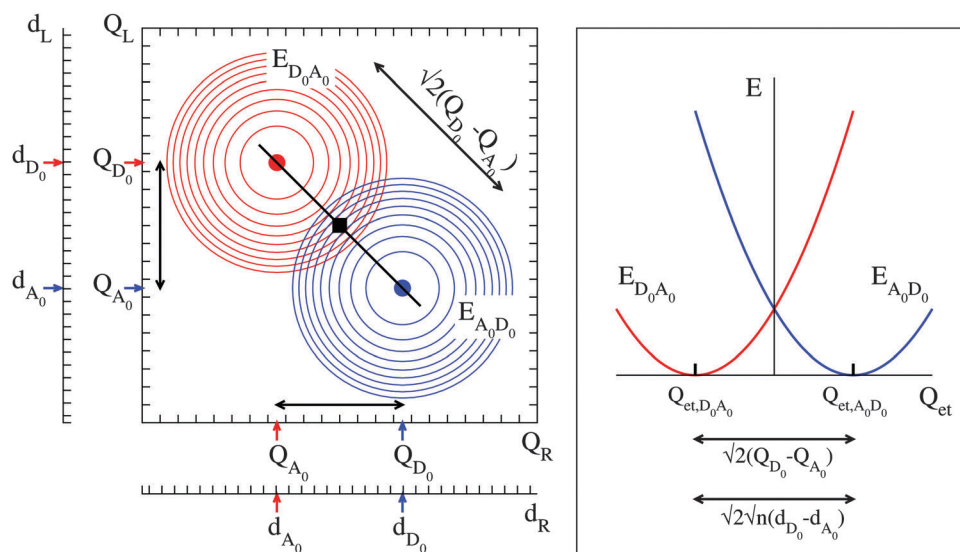


Fig. 2 Left: Ground state diabatic energy surfaces of the DA (red) and AD (blue) ionic configurations of the mixed valence pair. The black line that connects the DA minimum (red dot) with the AD minimum (blue dot) and passes through the activated complex (black square) is the electron transfer reaction coordinate, which is also the IVCT configuration coordinate. Right: IVCT configuration coordinate diagram with the ground state energies of DA (red) and AD (blue).

The diabatic potential energy surface $E_{A_0D_0}(Q_L, Q_R)$ is identical to $E_{D_0A_0}(Q_L, Q_R)$ but shifted $-(Q_{D_0} - Q_{A_0})$ in the Q_L axis and $+(Q_{D_0} - Q_{A_0})$ in the Q_R axis. They are represented in Fig. 2.

The crossing point between $E_{D_0A_0}$ and $E_{A_0D_0}$ with lowest energy is the activated complex (ac) of the thermal $DA \rightarrow AD$ electron transfer reaction at the diabatic level. Within the adopted approximations of identical D and A sites and a common force constant for both, this activated complex is at the midpoint between their respective minima: $Q_{L,ac} = Q_{R,ac} = Q_{ac} \equiv (Q_{D_0} + Q_{A_0})/2$. The electron transfer reaction coordinate is the straight line in the (Q_L, Q_R) plane that connects the $E_{D_0A_0}$ and $E_{A_0D_0}$ minima and passes through the activated complex,

$$\frac{Q_L - Q_{D_0}}{Q_R - Q_{A_0}} = -1. \quad (8)$$

Then, a normal electron transfer reaction coordinate Q_{et} can be defined as

$$Q_{et} = \frac{1}{\sqrt{2}}(Q_R - Q_L), \quad (9)$$

which is null for the activated complex, $Q_{et,ac} = 0$, and takes opposite values for the DA and AD ionic configurations at the equilibrium,

$$-Q_{et,D_0A_0} = Q_{et,A_0D_0} = \frac{1}{\sqrt{2}}(Q_{D_0} - Q_{A_0}), \quad (10)$$

which gives

$$Q_{et,A_0D_0} - Q_{et,D_0A_0} = \sqrt{2}(Q_{D_0} - Q_{A_0}). \quad (11)$$

Using the Q_{et} defined in eqn (9), the parametric form of the reaction coordinate is

$$\begin{cases} Q_L - Q_{ac} = -\frac{1}{\sqrt{2}}Q_{et}, \\ Q_R - Q_{ac} = +\frac{1}{\sqrt{2}}Q_{et}, \end{cases} \quad (12)$$

which makes it clear that an increase of Q_{et} means a simultaneous decrease of Q_L and an increase of Q_R . This reflects the fact that a thermal electron transfer from D_L to A_R , which converts D_LA_R into A_LD_R , is accompanied by a contraction of the coordination shells around the donor D_L and a simultaneous expansion around the acceptor A_R .

Accordingly, the energies of the two ionic configurations of the Yb^{2+}/Yb^{3+} mixed valence pair along the reaction coordinate are:

$$E_{D_0A_0}(Q_{et}) = \frac{1}{2}k(Q_{et} - Q_{et,D_0A_0})^2, \quad (13)$$

$$E_{A_0D_0}(Q_{et}) = \frac{1}{2}k(Q_{et} - Q_{et,A_0D_0})^2,$$

which are two identical parabolaes with a horizontal offset $\sqrt{2}(Q_{D_0} - Q_{A_0})$,

$$E_{D_0A_0}(Q_{et} - \sqrt{2}(Q_{D_0} - Q_{A_0})) = E_{A_0D_0}(Q_{et}). \quad (14)$$

Since the coordinate orthogonal to Q_{et} does not have a horizontal offset (Fig. 2), the reaction coordinate Q_{et} is the IVCT

configuration coordinate. The horizontal offset and the force constant k are the only two degrees of freedom of this model.

If Q_L and Q_R are the respective breathing modes of the Yb_L and Yb_R substitutional defects in YAG, which normally produce the maximum energy changes, they can be written as

$$\begin{aligned} Q_L &= \frac{1}{\sqrt{8}}(\delta_{O_{L_1}} + \delta_{O_{L_2}} + \dots + \delta_{O_{L_8}}), \\ Q_R &= \frac{1}{\sqrt{8}}(\delta_{O_{R_1}} + \delta_{O_{R_2}} + \dots + \delta_{O_{R_8}}), \end{aligned} \quad (15)$$

with $\delta_{O_{L_1}}$ being the increase of the $Yb_L-O_{L_1}$ distance with respect to its value in a given reference structure, and equivalently for the displacements of the other oxygen atoms. The electron transfer reaction coordinate Q_{et} defined in eqn (9) that corresponds to these definitions of Q_L and Q_R are shown in Fig. 3. Since all the Yb-O distances change equally during breathing, we can write

$$Q_L = \sqrt{8}(d_L - d_{ref}), \quad (16)$$

$$Q_R = \sqrt{8}(d_R - d_{ref}),$$

where d_{ref} , d_L , and d_R are, respectively, the average Yb-O distances in a reference structure, and around Yb_L and Yb_R at any moment. Then, for the donor and acceptor equilibrium structures we have

$$Q_{D_0} = \sqrt{8}(d_{D_0} - d_{ref}), \quad (17)$$

$$Q_{A_0} = \sqrt{8}(d_{A_0} - d_{ref}),$$

with d_{D_0} and d_{A_0} being the average Yb-O distances around the donor Yb^{2+} and the acceptor Yb^{3+} at equilibrium. In a more general case with a coordination number n of equal ligands,

$$Q_{D_0} = \sqrt{n}(d_{D_0} - d_{ref}), \quad (18)$$

$$Q_{A_0} = \sqrt{n}(d_{A_0} - d_{ref}).$$

This leads to the centers of the two parabolaes in the configuration coordinate diagram (eqn 13),

$$-Q_{et,D_0A_0} = Q_{et,A_0D_0} = \sqrt{n/2}(d_{D_0} - d_{A_0}), \quad (19)$$

and their offset

$$\sqrt{2}(Q_{D_0} - Q_{A_0}) = \sqrt{2n}(d_{D_0} - d_{A_0}). \quad (20)$$

Then, the horizontal offset (which is key to the model, together with the force constant) can be estimated from the difference

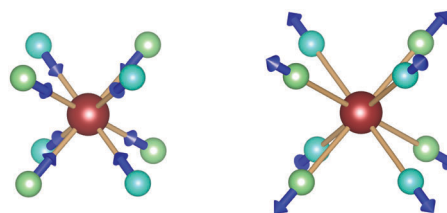


Fig. 3 Electron transfer reaction coordinate Q_{et} of an Yb^{2+}/Yb^{3+} pair in YAG.

between the ionic radii of the donor and acceptor ions, Yb^{2+} and Yb^{3+} in our working example.

The diabatic potential energy surfaces of other states of the $4f^N$ manifold of the $\text{Yb}^{2+}/\text{Yb}^{3+}$ mixed valence pair can be written as

$$E_{D_i A_j}(Q_L, Q_R) = E_{D_i A_j, e} + \frac{1}{2}k(Q_L - Q_{D_0})^2 + \frac{1}{2}k(Q_R - Q_{A_0})^2$$

$$E_{A_j D_i}(Q_L, Q_R) = E_{D_i A_j, e} + \frac{1}{2}k(Q_L - Q_{A_0})^2 + \frac{1}{2}k(Q_R - Q_{D_0})^2, \quad (21)$$

assuming that they have the same equilibrium structures and vibrational frequencies as the ground state. The vertical offsets $E_{D_i A_j, e}$ are the sum of the minimum-to-minimum excitation energies from the ground state to the i excited state of D and from the ground state to the j excited state of A: $E_{D_i A_j, e} = (E_{D_i, e} - E_{D_0, e}) + (E_{A_j, e} - E_{A_0, e})$. Those of the two complementary states $D_i A_j$ and $A_j D_i$ are identical: then, their energies in the IVCT configuration coordinate diagram are

$$E_{D_i A_j}(Q_{\text{et}}) = E_{D_i A_j, e} + \frac{1}{2}k(Q_{\text{et}} - Q_{\text{et}, D_0 A_0})^2,$$

$$E_{A_j D_i}(Q_{\text{et}}) = E_{D_i A_j, e} + \frac{1}{2}k(Q_{\text{et}} - Q_{\text{et}, A_0 D_0})^2. \quad (22)$$

In summary, eqn (22), together with eqn (19), or in a more general case with eqn (10), constitutes an IVCT configuration coordinate (diabatic) diagram of the D/A mixed valence pair.

The model of the potential energy surfaces can be improved by extending eqn (21). Using different force constants for D and A leads to a different electron transfer reaction coordinate but a configuration coordinate diagram like eqn (22) can still be used.⁹ In this case, the minima of DA and AD are not aligned with the activated complex and the reaction coordinate is made of two straight segments, one between DA and the activated complex and another between the activated complex and AD. Also, using state-specific equilibrium structures, or state-specific force constants, or including anharmonic terms, will prevent from defining a unique reaction coordinate, because there is a different one for each $D_i A_j - A_k D_l$ combination. In the case of excited states of a different configuration, like $4f^{N-1}5d$, using state-specific equilibrium structures, or at least configuration-specific equilibrium structures, might be necessary. If so, the one-dimension configuration coordinate diagram will break in a strict sense and working with the two-dimension energy surfaces is compulsory. However, the reaction coordinates of several $D_i A_j - A_k D_l$ combinations can be similar enough so as to make the representation of all states of the mixed valence pair along one of these reaction coordinates meaningful.⁹

B. IVCT configuration coordinate diagram of $\text{Yb}^{2+}/\text{Yb}^{3+}$ in YAG

In Fig. 4 we show the IVCT configuration coordinate diagram of the $4f^N$ levels of an $\text{Yb}^{2+}/\text{Yb}^{3+}$ mixed valence pair in YAG. It results from using eqn (19) and (22) with $n = 8$ and the following data: (1) the $E_{D_i A_j, e}$ are the experimental $4f \rightarrow 4f$ excitation energies of Yb^{3+} , which are shown in the second column of Table 1 (note that Yb^{2+} has only one state of the $4f^{14}$ configuration).

(2) For the $d_{D_0} - d_{A_0}$ offset between donor and acceptor equilibrium distances, which is $d_{\text{Yb}^{2+}-\text{O}} - d_{\text{Yb}^{3+}-\text{O}}$, we have taken 90% of the difference between the ionic radii of Yb^{2+} and Yb^{3+} in coordination 8 (1.14 Å and 0.985 Å respectively, ref. 18), which is $d_{D_0} - d_{A_0} = 0.14$ Å. The reduction factor has been used to take into account the host effect, which has been found to lie between the cation–ligand distance in the undoped host and the distance that would correspond to the ionic radii mismatch between the host cation and the impurity.¹⁹ (3) The force constant is $k = \mu\omega^2$, with $\mu = m(\text{O}) = 15.999$ amu. We are not aware of the direct experimental determinations of the breathing mode vibrational frequency of Yb^{3+} defects in YAG; we have taken a $\bar{\nu} = \omega/(2\pi c) = 326$ cm^{-1} mode reported by Lupei *et al.*²⁰ after an analysis of resonant vibronic effects in YAG: Yb^{3+} and have scaled it 0.95% down to 310 cm^{-1} . This corresponds to a 90% scaling of the force constant k , which is expected to be smaller in Yb^{2+} than in Yb^{3+} . Since

$$\frac{k}{\text{cm}^{-1} \text{Å}^{-2}} = 0.029660 \times \left(\frac{\mu}{\text{amu}}\right) \times \left(\frac{\bar{\nu}}{\text{cm}^{-1}}\right)^2,$$

we get $k = 50\,434$ $\text{cm}^{-1} \text{Å}^{-2}$.

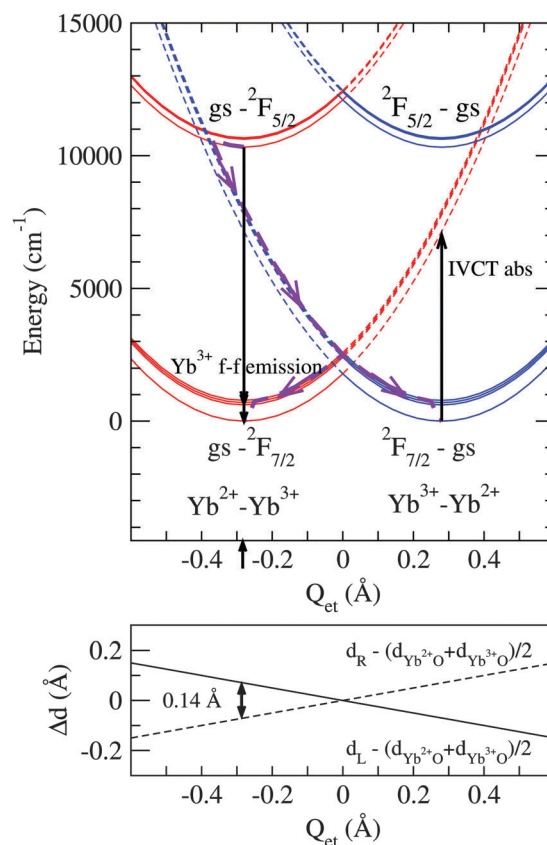


Fig. 4 Top: IVCT configuration coordinate diagram of a $\text{Yb}^{2+}/\text{Yb}^{3+}$ mixed valence pair in YAG. Bottom: Changes of the Yb–O distance in the left Yb (d_L , full line) and right Yb (d_R , dashed line) with respect to their value at the activated complex, $(d_{\text{Yb}^{2+}-\text{O}, e} + d_{\text{Yb}^{3+}-\text{O}, e})/2$, along the configuration coordinate (or electron transfer reaction coordinate) Q_{et} .

In the IVCT configuration coordinate diagram (Fig. 4) we observe the energies of the seven levels of the $\text{Yb}_L^{2+}\text{-Yb}_R^{3+}$ (in red) and the seven levels of the $\text{Yb}_L^{3+}\text{-Yb}_R^{2+}$ (in blue) ionic configurations of the pair. They are grouped in two sets of four levels corresponding to $\text{Yb}_R^{3+}(^2F_{7/2})$ and $\text{Yb}_L^{3+}(^2F_{7/2})$, and two sets of three levels about $10\,000\text{ cm}^{-1}$ above, corresponding to $\text{Yb}_R^{3+}(^2F_{5/2})$ and $\text{Yb}_L^{3+}(^2F_{5/2})$. They have been represented with full lines for configuration coordinate values around their respective minima. We used dashed lines for their energies at configuration coordinate values corresponding to stressed structures. For instance, at $Q_{\text{et}} = -0.28\text{ \AA}$ we find $\text{Yb}_L^{2+}\text{-Yb}_R^{3+}$ in equilibrium (full lines), with a long $\text{Yb}_L\text{-O}$ distance and a short $\text{Yb}_R\text{-O}$ distance; in contrast, an $\text{Yb}_L^{3+}\text{-Yb}_R^{2+}$ state is under strong stress in such a structure (dashed lines) and it will relax towards a short $\text{Yb}_L\text{-O}$ distance and a long $\text{Yb}_R\text{-O}$ distance, increasing Q_{et} and releasing a large reorganization energy (about 7500 cm^{-1}). It is clear that structurally stressed IVCT states intercalate between states of the pairs around their equilibrium. Vertical (Frank-Condon) transitions between full lines take place in Yb^{3+} . Vertical transitions between full and dashed lines are IVCT transitions; they end in structurally stressed states and take place between states with large horizontal offsets, which produces very broad bands. IVCT absorptions in mixed valence compounds have long been known;^{5,6} they take place without a corresponding emission. IVCT emissions from higher excited states have been recently reported in mixed valence dopant pairs in solids. They have been found to be responsible for the anomalous emission of Ce^{3+} -doped elpasolites⁹ and for the interplay between anomalous emissions and $5d \rightarrow 4f$ emissions in Yb -doped fluorite hosts.¹⁰ The IVCT emissions have large Stokes shifts associated with large reorganization energies.

It is interesting to observe in the IVCT configuration coordinate diagram that IVCT crossings between the excited $\text{Yb}_L^{2+}\text{-Yb}_R^{3+}(^2F_{5/2})$ and the ground $\text{Yb}_L^{3+}(^2F_{7/2})\text{-Yb}_R^{2+}$ manifolds can occur with low energy barriers. Obviously, the same is true for their symmetrical counterparts. With the present data we obtain a 200 cm^{-1} energy barrier from the minimum of the $\text{Yb}_L^{2+}\text{-Yb}_R^{3+}(^2F_{5/2})$ state (which is the emitting state of the $\text{Yb}^{3+} 4f \rightarrow 4f$ emission) to the crossing between the lowest $\text{Yb}_L^{2+}\text{-Yb}_R^{3+}(^2F_{5/2})$ level and the highest $\text{Yb}_L^{3+}(^2F_{7/2})\text{-Yb}_R^{2+}$ level. This result suggests the consideration of the nonradiative $\text{Yb}^{2+}(4f_{7/2}) \rightarrow \text{Yb}^{3+}(4f_{5/2})$ electron transfer in $\text{Yb}^{2+}/\text{Yb}^{3+}$ pairs as a possible mechanism responsible for quenching of the Yb^{3+} emission, which is shown in violet in Fig. 4. This means that $\text{Yb}^{2+}/\text{Yb}^{3+}$ pairs can be the active quenchers in the concentration quenching of the Yb^{3+} emission.²¹ Also, they can explain the temperature quenching of the Yb^{3+} emission excited with $\text{Ce}^{3+} 4f \rightarrow 5d$ absorption in Ce, Yb -codoped YAG.³

The uncertainties of the empirical data used to build the configuration coordinate diagram in Fig. 4 give only a qualitative or semi-quantitative meaning to the energy barrier just discussed. For instance, taking 95% or 85% of the ionic radii difference for $d_{\text{Yb}^{2+}\text{-O}} - d_{\text{Yb}^{3+}\text{-O}}$ instead of 90%, leads to 75 cm^{-1} and 400 cm^{-1} energy barriers instead of the 200 cm^{-1} mentioned above. Similarly, using a higher/lower vibrational frequency would decrease/increase the barrier value in this case. Besides, the

effective activation energies that are experimentally determined are smaller than the barrier energies calculated from configuration coordinate diagrams because of the effective overlap between vibrational wavefunctions below the crossing points.²² Nevertheless, it is clear that a configuration coordinate diagram obtained with reasonable empirical data indicates that a crossing between a potentially emitting level $\text{Yb}_L^{2+}\text{-Yb}_R^{3+}(^2F_{5/2})$ and a structurally stressed IVCT ground state level $\text{Yb}_L^{3+}(^2F_{7/2})\text{-Yb}_R^{2+}$ is likely to occur and it would cause thermal quenching of the $\text{Yb}^{3+} 4f \rightarrow 4f$ emission.

IV. MMCT configuration coordinate diagram of a metal–metal pair

In this section, we describe the configuration coordinate diagram of the metal-to-metal charge transfer states of a pair of ions of different elements in a solid host. We will take a $\text{Ce}^{3+}\text{-Yb}^{3+}$ pair in Ce, Yb -codoped YAG as a working example. We assume Ce^{3+} and Yb^{3+} substitute for Y at a D_2 symmetry site with 8-fold oxygen coordination. Regarding Ce^{3+} , we will focus on its states of the $4f^1$ configuration and on its lowest $5d^1$ state. As is shown in Table 1, the seven $4f^1$ states are grouped in three sets:^{15,16} a first set with three levels spanning about 800 cm^{-1} , 1–3 Γ_5 ; a second set starting at about 2100 cm^{-1} above the ground state with three levels spanning at 350 cm^{-1} , 4–6 Γ_5 ; and a third set at about 3800 cm^{-1} above the ground state with one level, 7 Γ_5 . (This distribution of levels differs from the extended assumption of three $^2F_{5/2}$ related levels and four $^2F_{7/2}$ related levels separated by about 2500 cm^{-1} ; a $4f$ crystal field splitting of the same size of the $4f$ spin-orbit coupling splitting is responsible for the partial break of such assumption.¹⁶) The lowest $5d^1$ state is $20\,450\text{ cm}^{-1}$ above the ground state.¹⁷ These levels will combine with the previously described four $^2F_{7/2}$ related levels and three $^2F_{5/2}$ related levels of Yb^{3+} (Section III). The result of this combination is four main sets of levels. A first main set of 28 levels of the $\text{Ce}^{3+}(4f^1)\text{-Yb}^{3+}(^2F_{7/2})$ character lies between 0 and 4600 cm^{-1} and is divided in three subsets: $12\text{Ce}^{3+}(1\text{--}3\ \Gamma_5)\text{-Yb}^{3+}(^2F_{7/2})$, $12\text{Ce}^{3+}(4\text{--}6\ \Gamma_5)\text{-Yb}^{3+}(^2F_{7/2})$, and $4\text{Ce}^{3+}(7\ \Gamma_5)\text{-Yb}^{3+}(^2F_{7/2})$. A second main set of 21 levels of the $\text{Ce}^{3+}(4f^1)\text{-Yb}^{3+}(^2F_{5/2})$ character lies between $10\,300\text{ cm}^{-1}$ and $14\,500\text{ cm}^{-1}$ and is divided in three subsets: $9\text{Ce}^{3+}(1\text{--}3\ \Gamma_5)\text{-Yb}^{3+}(^2F_{5/2})$, $9\text{Ce}^{3+}(4\text{--}6\ \Gamma_5)\text{-Yb}^{3+}(^2F_{5/2})$, and $3\text{Ce}^{3+}(7\ \Gamma_5)\text{-Yb}^{3+}(^2F_{5/2})$. A third main set of 4 levels of $\text{Ce}^{3+}(5d_1^1)\text{-Yb}^{3+}(^2F_{7/2})$ character lies between $20\,450\text{ cm}^{-1}$ and $21\,230\text{ cm}^{-1}$. Finally a fourth main set of 4 levels of the $\text{Ce}^{3+}(5d_1^1)\text{-Yb}^{3+}(^2F_{5/2})$ character lies between $30\,770\text{ cm}^{-1}$ and $31\,120\text{ cm}^{-1}$. Between the third and the fourth set, states of $\text{Ce}^{3+}(5d_2^1)\text{-Yb}^{3+}(^2F_{7/2})$ character associated with the second $5d^1$ excited state of Ce^{3+} may appear. Here we will only pay attention to the three first sets.

Electron transfer from Ce^{3+} to Yb^{3+} results into a $\text{Ce}^{4+}\text{-Yb}^{2+}$ pair with a closed-shell ground state much more stable than all its excited states. This level may lie between the $\text{Ce}^{3+}\text{-Yb}^{3+}$ states just discussed. Such a consideration has led to propose its involvement in the mechanism of energy transfer from Ce^{3+} to Yb^{3+} in Ce, Yb -codoped YAG, as well as in the quenching of

the Ce^{3+} -excited Yb^{3+} -emission of this material.³ The question we tackle here is how to represent the energies of the levels of the Ce^{3+} - Yb^{3+} and Ce^{4+} - Yb^{2+} pairs together in a simplified diagram, which is called the MMCT configuration coordinate diagram.

A. MMCT model

In order to make the notation more general, we will call Ce^{3+} the donor D and Yb^{3+} the acceptor A. After the electron transfer they result into Ce^{4+} and Yb^{2+} , which will be respectively called D^+ and A^- . As in the IVCT case, D, A, D^+ , and A^- refer to the defect centers the respective ions create in the solid, which will be atomic moieties containing at least their first coordination shells, rather than to the single ions. Then, the pair Ce^{3+} - Yb^{3+} is DA and the pair Ce^{4+} - Yb^{2+} is D^+A^- .

We aim at describing the energies of the states of the Ce^{3+} - Yb^{3+} and Ce^{4+} - Yb^{2+} pairs (DA and D^+A^-) as functions of two vibrational coordinates Q_D and Q_A , which describe vibrations of the moieties containing Ce (D and D^+) and Yb (A and A^-) respectively. Note that in MMCT, contrary to IVCT, D and D^+ refer to a different element than A and A^- , so that there is no need to use the *left* and *right* atoms to differentiate them; in other words, Ce is always the *left* atom and Yb the *right* atom. This is why we use Q_D and Q_A here instead of Q_L and Q_R . As in IVCT, Q_D and Q_A can be the configuration coordinate described in Section II of the Ce and Yb active centers, but they can also be other totally symmetric vibrational coordinates of these centers.

The diabatic energy of the ground state of the DA pair, as a function of the positions of the ligands that can be described using the coordinates Q_D and Q_A , can be written as

$$E_{D_0A_0}(Q_D, Q_A) = \frac{1}{2}k_D(Q_D - Q_{D_0})^2 + \frac{1}{2}k_A(Q_A - Q_{A_0})^2, \quad (23)$$

in a quadratic approximation. Q_{D_0} and Q_{A_0} are the values of the vibrational coordinates of the donor and acceptor moieties at the respective equilibrium structures of D and A. $k_D = \mu_D\omega_D^2$ and $k_A = \mu_A\omega_A^2$ are, respectively, the donor and acceptor force constants, μ_D and μ_A their vibrational masses, and ω_D and ω_A their vibrational frequencies. As in IVCT, using this equation we are establishing the ground state energy of the DA pair at its minimum as the reference energy.

The diabatic energy of the ground state of the D^+A^- pair that results after MMCT from DA can be written as

$$E_{D_0^+A_0^-}(Q_D, Q_A) = E_{D_0^+A_0^-,e} + \frac{1}{2}k_D(Q_D - Q_{D_0^+})^2 + \frac{1}{2}k_A(Q_A - Q_{A_0^-})^2. \quad (24)$$

Here, as in the IVCT model of Section III, we assume a common force constant k_D for D and D^+ on one side, and k_A for A and A^- on the other; $Q_{D_0^+}$ and $Q_{A_0^-}$ are the values of the vibrational coordinates of the donor and acceptor moieties at the respective equilibrium structures of D^+ and A^- . $E_{D_0^+A_0^-,e}$ is the vertical offset between the minima of the D^+A^- and DA ground state potential energy surfaces. In an empirical approach to the problem, it can be considered an empirical parameter. Also, it might eventually be convenient to regard it as the sum of: (1) the adiabatic

ionization potential of D in the host, IP_D (energy difference between the ground states of D^+ and D at their relaxed structures), (2) the negative adiabatic electron affinity of A in the host, $-EA_A$ (energy difference between the ground states of A^- and A at their relaxed structures), and (3) the interaction energy change due to the creation of a hole in D and an electron in A; for long D-A separations, this can be approximated by $(q_A - q_D - 1)/d_{DA}$, with d_{DA} being the distance between the donor and the acceptor, and q_D and q_A their respective defect charges:

$$E_{D_0^+A_0^-,e} = IP_D - EA_A + (q_A - q_D - 1)/d_{DA}. \quad (25)$$

The $E_{D_0A_0}(Q_D, Q_A)$ and $E_{D_0^+A_0^-}(Q_D, Q_A)$ potential energy surfaces are represented on the left hand side of Fig. 5.

Within these approximations, the activated complex of the thermal $DA \rightarrow D^+A^-$ reaction is in the straight line that connects their minima. Its exact position depends on the value of the energy offset $E_{D_0^+A_0^-,e}$. In any case, as in the IVCT case, the electron transfer reaction coordinate is the straight line in the (Q_D, Q_A) plane that passes through the $E_{D_0A_0}$ and $E_{D_0^+A_0^-}$ minima,

$$\frac{Q_D - Q_{D_0}}{Q_A - Q_{A_0}} = m \equiv \frac{Q_{D_0^+} - Q_{D_0}}{Q_{A_0^-} - Q_{A_0}}. \quad (26)$$

with a negative slope m . Then, a normal reaction coordinate could be defined like in eqn (9), which would be null in the activated complex. However, since the position of the activated complex can be very different for different pairs of DA and D^+A^- states, it can be more convenient to define here the normal reaction coordinate so that it is null for the DA ground state at equilibrium:

$$Q_{et} = \frac{1}{\sqrt{1+m^2}}[(Q_A - Q_{A_0}) + m(Q_D - Q_{D_0})]. \quad (27)$$

Then, the parametric form of the reaction coordinate is

$$\begin{cases} Q_D - Q_{D_0} = \frac{m}{\sqrt{1+m^2}}Q_{et}, \\ Q_A - Q_{A_0} = \frac{1}{\sqrt{1+m^2}}Q_{et}. \end{cases} \quad (28)$$

which, with a negative m , indicates that an increase of Q_{et} means a simultaneous decrease of Q_D and an increase of Q_A .

Being the only coordinate with a horizontal offset, Q_{et} is the MMCT configuration coordinate and the energies of the ground states of the Ce^{3+} - Yb^{3+} and Ce^{4+} - Yb^{2+} pairs as functions of it constitute the configuration coordinate diagram for these states. Using eqn (23), (24) and (28), they are:

$$E_{D_0A_0}(Q_{et}) = \frac{1}{2}k_D(Q_{et} - Q_{et,D_0A_0})^2 \quad (29)$$

$$E_{D_0^+A_0^-}(Q_{et}) = E_{D_0^+A_0^-,e} + \frac{1}{2}k_{et}(Q_{et} - Q_{et,D_0^+A_0^-})^2,$$

with

$$Q_{et,D_0A_0} = 0 \quad (30)$$

$$Q_{et,D_0^+A_0^-} = \sqrt{(Q_{D_0} - Q_{D_0^+})^2 + (Q_{A_0^-} - Q_{A_0})^2},$$

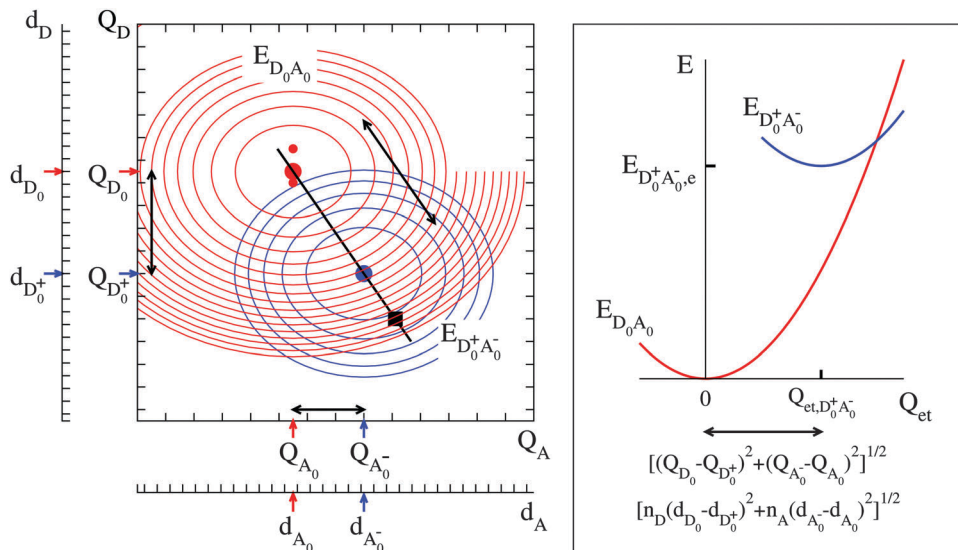


Fig. 5 Left: Ground state diabatic energy surfaces of DA (red) and D^+A^- (blue). The black line that connects the DA minimum (red dot) with the activated complex (black square) and returns to the D^+A^- minimum (blue dot) is the electron transfer reaction coordinate, which is also the MMCT configuration coordinate. The minima of other two DA energy surfaces (not represented here) are indicated with red dots. Right: MMCT configuration coordinate diagram with the ground state energies of DA (red) and D^+A^- (blue).

and

$$k_{\text{ct}} = \frac{1}{1+m^2}(m^2k_D + k_A). \quad (31)$$

The MMCT configuration coordinate diagram with $E_{D_0A_0}(Q_{\text{ct}})$ and $E_{D_0^+A_0^-}(Q_{\text{ct}})$ is represented on the right hand side of Fig. 5. The three degrees of freedom of this MMCT configuration coordinate diagram are the electron transfer reaction coordinate curvature, k_{ct} , the MMCT horizontal offset $\sqrt{(Q_{D_0} - Q_{D_0^+})^2 + (Q_{A_0} - Q_{A_0^-})^2}$, and the vertical offset $E_{D_0^+A_0^-}$.

If Q_D and Q_A are the breathing modes of the donor and the acceptor, with n_D and n_A equal ligands, respectively, we have

$$\begin{aligned} Q_{D_0} - Q_{D_0^+} &= \sqrt{n_D}(d_{D_0} - d_{D_0^+}), \\ Q_{A_0^-} - Q_{A_0} &= \sqrt{n_A}(d_{A_0^-} - d_{A_0}), \end{aligned} \quad (32)$$

and a horizontal offset

$$\begin{aligned} Q_{\text{ct},D_0^+A_0^-} - Q_{\text{ct},D_0A_0} &= Q_{\text{ct},D_0^+A_0^-} \\ &= \sqrt{n_D(d_{D_0} - d_{D_0^+})^2 + n_A(d_{A_0^-} - d_{A_0})^2}. \end{aligned} \quad (33)$$

For excited states of DA and D^+A^- , the diabatic energy surfaces are

$$\begin{aligned} E_{D_iA_j}(Q_D, Q_A) &= E_{D_iA_j,e} + \frac{1}{2}k_D(Q_D - Q_{D_i})^2 + \frac{1}{2}k_A(Q_A - Q_{A_j})^2, \\ E_{D_k^+A_\ell^-}(Q_D, Q_A) &= E_{D_k^+A_\ell^-,e} + \frac{1}{2}k_D(Q_D - Q_{D_k^+})^2 \\ &\quad + \frac{1}{2}k_A(Q_A - Q_{A_\ell^-})^2. \end{aligned} \quad (34)$$

The energy offsets of DA are the sums of the minimum-to-minimum excitation energies from the ground state to the i excited state of D and from the ground state to the j excited state of A: $E_{D_iA_j,e} = (E_{D_i,e} - E_{D_0,e}) + (E_{A_j,e} - E_{A_0,e})$. Correspondingly, the energy offsets of D^+A^- are the sums of the minimum-to-minimum excitation energies from the ground state to the k excited state of D^+ and from the ground state to the ℓ excited state of A^- , plus the ground state energy offset $E_{D_0^+A_0^-}$, which fulfils eqn (25): $E_{D_k^+A_\ell^-,e} = E_{D_0^+A_0^-} + (E_{D_k^+,e} - E_{D_0^+,e}) + (E_{A_\ell^-,e} - E_{A_0^-,e})$. The D^+A^- ground state energy offset $E_{D_0^+A_0^-}$ is the only parameter of the model that depends on the donor-acceptor distance d_{DA} . This means that when two or more DA pairs made of the same elements coexist in the same host with different D-A distances, d_{DA} and $d_{DA'}$, their MMCT manifolds $E_{D_k^+A_\ell^-}$ are identical and shifted in energy with respect to one another. Eqn (25) gives $(q_A - q_D - 1)(1/d_{DA} - 1/d_{DA'})$ for the shift.

In general, there will be one reaction coordinate for each D_iA_j - $D_k^+A_\ell^-$ combination. However, if the horizontal offsets between different states of DA are much smaller than the MMCT horizontal offset, it is not a bad approximation to use the ground state reaction coordinate eqn (27) for all the states. In this case, we have

$$\begin{aligned} E_{D_iA_j}(Q_{\text{ct}}) &= E_{D_iA_j,e} + \frac{1}{2}k_{\text{ct}}(Q_{\text{ct}} - Q_{\text{ct},D_0A_0})^2 \\ E_{D_k^+A_\ell^-}(Q_{\text{ct}}) &= E_{D_k^+A_\ell^-,e} + \frac{1}{2}k_{\text{ct}}(Q_{\text{ct}} - Q_{\text{ct},D_0^+A_0^-})^2. \end{aligned} \quad (35)$$

Summarizing, eqn (35), together with eqn (33), or in a more general case with eqn (30), constitutes the MMCT configuration coordinate (diabatic) diagram of the DA and D^+A^- metal-metal pairs in a host.

Alternatively, if the horizontal offsets between different states of either DA or D^+A^- are taken into account, then the

MMCT configuration coordinate diagram results from evaluating eqn (34) along the reaction coordinate of eqn (26), (27) and (32). If the reaction coordinate of a set of excited states $D_iA_j - D_k^+A_l^-$ is taken as the configuration coordinate, instead of the ground state combination $D_0A_0 - D_0^+A_0^-$, then, eqn (26) and (27) are still valid to define such a coordinate, as long as Q_{D_0} , Q_{A_0} , $Q_{D_0^+}$, and $Q_{A_0^-}$, are substituted by the corresponding Q_{D_i} , Q_{A_j} , $Q_{D_k^+}$, and $Q_{A_l^-}$.

B. MMCT configuration coordinate diagram of Ce^{3+}/Yb^{3+} in YAG

In Fig. 6 we show a MMCT configuration coordinate diagram of Ce^{3+}/Yb^{3+} in YAG, which results from representing eqn (34) along the ground state electron transfer reaction coordinate defined by eqn (26), (27), and (32). The representation along the $Ce^{3+}(5d_1^1) - Yb^{3+}(^2F_{7/2}) \rightarrow Ce^{4+} - Yb^{2+}$ reaction coordinate in the same scale is hard to distinguish at sight. We used the following data: (1) the $E_{D_iA_j,e} = E_e(Ce_i^{3+} - Yb_j^{3+})$ energy offsets were obtained from the experimental excitation energies of Ce^{3+} and Yb^{3+} , which are shown in Table 1. Since we do not have empirical data on the minimum-to-minimum Ce^{3+} -to- Yb^{3+} charge transfer excitation energy, we treat it here as an empirical parameter such that it provides a diagram consistent with the experiments; hence, we used $E_{D_0^+A_0^-,e} = E_e(Ce^{4+} - Yb^{2+}) = 14\,000\text{ cm}^{-1}$. (2) We used $d_{A_0^-} - d_{A_0} = d_{Yb^{2+}O} - d_{Yb^{3+}O} = 0.14\text{ \AA}$, as in Section III.B, and

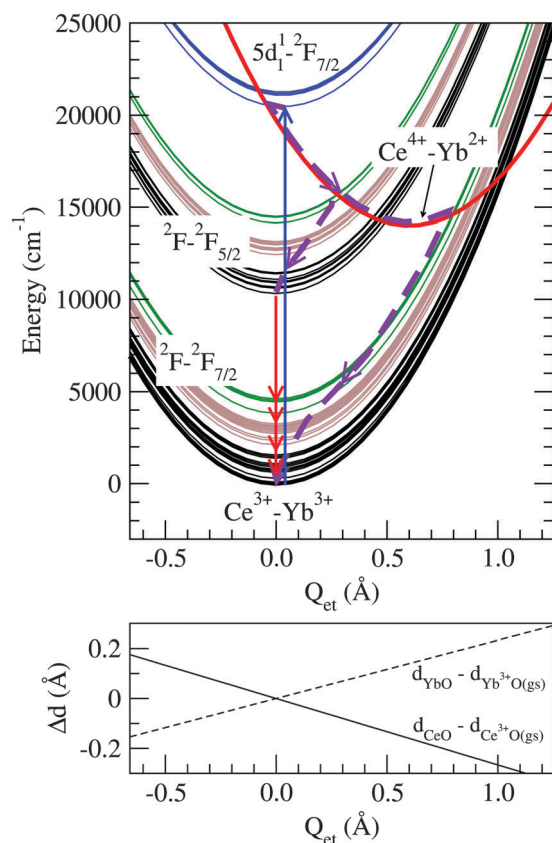


Fig. 6 MMCT configuration coordinate diagram of Ce^{3+}/Yb^{3+} pairs in YAG. The following processes are indicated: Ce^{3+} lowest $4f \rightarrow 5d$ absorption (blue arrow); energy transfer to the $^2F_{5/2}$ excited state of Yb^{3+} and non-radiative decay to the ground states of Ce^{3+} and Yb^{3+} through the $Ce^{4+}-Yb^{2+}$ MMCT state (dashed violet line); and $Yb^{3+}4f \rightarrow 4f$ emission (red arrows).

$d_{D_0^-} - d_{D_0^+} = d_{Ce^{3+}O} - d_{Ce^{4+}O} = 0.16\text{ \AA}$, using the same procedure as in Yb^{2+}/Yb^{3+} (90% of the difference between the ionic radii of Ce^{3+} and Ce^{4+} in coordination 8, 1.143 \AA and 0.97 \AA respectively.¹⁸). We used the same Ce–O distance offset in all $4f^1$ states of Ce^{3+} and a -0.02 \AA offset for the lowest $5d^1$ state (Table 1), slightly larger than the -0.014 \AA found in *ab initio* calculations in YAG: Ce^{3+} , which has been considered to be underestimated.²³ (3) The donor and acceptor force constants are $k_D = \mu\omega_D^2$ and $k_A = \mu\omega_A^2$, with $\mu = m(O) = 15.999\text{ amu}$. We used $\bar{\nu}_D = \omega_D/(2\pi c) = 210\text{ cm}^{-1}$, which is 5% larger than the 200 cm^{-1} vibrational sequence found in ref. 17 for YAG: Ce^{3+} (it corresponds to using a common force constant for Ce^{3+} and Ce^{4+} 10% larger than that of Ce^{3+} ; the force constant is expected to be larger in Ce^{4+} than in Ce^{3+}). And we used $\bar{\nu}_A = \omega_A/(2\pi c) = 310\text{ cm}^{-1}$, which is the common vibrational frequency for Yb^{2+} and Yb^{3+} that we used in Section III.B.

In the MMCT configuration coordinate diagram, we observe the states of the $Ce^{3+}-Yb^{3+}$ pair, which have been discussed above, and, crossing them, the ground state of the $Ce^{4+}-Yb^{2+}$ pair, with a horizontal offset of 0.60 \AA (eqn (33)). This diagram is basically consistent with the experiments and the interpretations given in ref. 3. The lowest $Ce^{3+}(5d_1^1) - Yb^{3+}(^2F_{7/2})$ state can decay nonradiatively to the $Ce^{4+}-Yb^{2+}$ MMCT state with a small energy barrier. This barrier is 73 cm^{-1} and the crossing is produced on the left side of the $Ce^{3+}(5d_1^1) - Yb^{3+}(^2F_{7/2})$ minimum with the above data; although the energy of the barrier can change with the parameters of the model, the basic interpretation is maintained for a relatively wide range around the present data. Next, the $Ce^{4+}-Yb^{2+}$ MMCT state can decay directly to the $Ce^{3+}(4f^1) - Yb^{3+}(^2F_{5/2})$ manifold, which can yield $Yb^{3+}^2F_{5/2} \rightarrow ^2F_{7/2}$ emission. This is consistent with the observations of energy transfer from Ce^{3+} to Yb^{3+} in YAG:Ce,Yb, with its temperature dependence, and with the Yb^{3+} emission not showing rise time, so that it supports the given interpretation as due to a thermally activated decay through an intermediate $Ce^{4+}-Yb^{2+}$ charge transfer state,³ and complements it with a more detailed description. A value of $E_e(Ce^{4+}-Yb^{2+})$ around 2000 cm^{-1} higher is also consistent with the experiments: *e.g.* a value of $16\,000\text{ cm}^{-1}$ gives a 30 cm^{-1} barrier and a crossing on the right side of the minimum. Note that according to eqn (25), several $E_e(Ce^{4+}-Yb^{2+})$ values associated to different Ce–Yb distances can coexist in the material.

An additional interesting feature was observed in the experiments of ref. 3: the intensity of the $Yb^{3+}4f \rightarrow 4f$ emission as excited with the $Ce^{3+}4f \rightarrow 5d$ absorption strongly decreases above 110 K, after the initial increase with temperature due to the thermally activated crossing to the $Ce^{4+}-Yb^{2+}$ MMCT state. The crossing between the $Ce^{4+}-Yb^{2+}$ MMCT state and the lowest $Ce^{3+}(4f^1) - Yb^{3+}(^2F_{7/2})$ manifold was suggested as a possible explanation. The present MMCT configuration coordinate diagram does not rule out such an explanation because the crossing exists, although it has a relatively high barrier (590 cm^{-1} with the present data). However, the consideration of both, the MMCT diagram of $Ce^{3+}-Yb^{3+}$ in YAG (Fig. 6) and the IVCT diagram of $Yb^{2+}-Yb^{3+}$ in YAG (Fig. 4), suggests an alternative explanation: the Ce^{3+} -to- Yb^{3+} MMCT produced after the $Ce^{3+}4f \rightarrow 5d$ absorption increases the probability of formation of $Yb^{2+}-Yb^{3+}$ pairs, hence, of quenching

the $\text{Yb}^{3+} 4f \rightarrow 4f$ emission *via* IVCT non-radiative decay, as discussed in Section III.B.

V. Conclusions

Quantitative configuration coordinate diagrams for intervalence charge transfer states of mixed valence pairs and metal-to-metal charge transfer states of heteronuclear pairs of dopant ions in solid hosts have been introduced and discussed in detail. They are obtained with the use of vibrational frequencies and excitation energies of single-ion active centers, together with differences between ion–ligand distances of the single-ion donor and acceptor centers. These data are attainable empirically, either from direct measurements or from estimations, *e.g.* based on ionic radii, and they can be calculated using *ab initio* methods. The IVCT configuration coordinate diagram of the $\text{Yb}^{2+}/\text{Yb}^{3+}$ mixed valence pair in Yb-doped YAG, and the MMCT configuration coordinate diagram of the $\text{Ce}^{3+}/\text{Yb}^{3+}$ heteronuclear pair in Ce,Yb-codoped YAG have been obtained and discussed. Empirical data of the individual ions doped in YAG have been used for this purpose.

The analysis of the $\text{Yb}^{2+}/\text{Yb}^{3+}$ IVCT diagram suggests that quenching of the $\text{Yb}^{3+} 4f \rightarrow 4f$ emission takes place by means of IVCT non-radiative decay in $\text{Yb}^{2+}/\text{Yb}^{3+}$ pairs.

The analysis of the $\text{Ce}^{3+}/\text{Yb}^{3+}$ MMCT diagram supports a previous interpretation of energy transfer from Ce^{3+} to Yb^{3+} in Ce,Yb-codoped YAG, after $\text{Ce}^{3+} 4f \rightarrow 5d$ excitation, *via* a $\text{Ce}^{4+}-\text{Yb}^{2+}$ MMCT state. The diagram provides the details of this process. The energy of the structurally relaxed $\text{Ce}^{4+}-\text{Yb}^{2+}$ pair is estimated to lie at either about $14\,000\text{ cm}^{-1}$ or $16\,000\text{ cm}^{-1}$ above the structurally relaxed $\text{Ce}^{3+}-\text{Yb}^{3+}$ pair. According to the diagram, there is a higher probability of nonradiative decay from the intermediate $\text{Ce}^{4+}-\text{Yb}^{2+}$ pair to the excited $\text{Ce}^{3+}(4f^1)-\text{Yb}^{3+}(^2F_{5/2})$ manifold than to the ground $\text{Ce}^{3+}(4f^1)-\text{Yb}^{3+}(^2F_{7/2})$ manifold of the $\text{Ce}^{3+}-\text{Yb}^{3+}$ pair. Altogether, the two diagrams suggest that the temperature quenching of the $\text{Yb}^{3+} 4f \rightarrow 4f$ emission excited with $\text{Ce}^{3+} 4f \rightarrow 5d$ absorption is due to the formation of $\text{Yb}^{2+}-\text{Yb}^{3+}$ pairs after MMCT from Ce^{3+} -to- Yb^{3+} in $\text{Ce}^{3+}-\text{Yb}^{3+}$ pairs.

Acknowledgements

This work was partly supported by a grant from Ministerio de Economía y Competitividad, Spain (Dirección General de Investigación

y Gestión del Plan Nacional de I+D+I, MAT2011-24586 and MAT2014-54395-P).

References

- 1 J. W. Verhoeven, *Pure Appl. Chem.*, 1996, **68**, 2223.
- 2 G. Blasse, *Struct. Bonding*, 1991, **76**, 153.
- 3 D. C. Yu, F. T. Rabouw, W. Q. Boon, T. Kieboom, S. Ye, Q. Y. Zhang and A. Meijerink, *Phys. Rev. B: Condens. Matter Mater. Phys.*, 2014, **90**, 165126.
- 4 E. Pinel, P. Boutinaud and R. Mahiou, *J. Alloys Compd.*, 2004, **380**, 225.
- 5 G. C. Allen and N. S. Hush, *Prog. Inorg. Chem.*, 1967, **8**, 357.
- 6 M. Robin and P. Day, *Adv. Inorg. Chem. Radiochem.*, 1968, **10**, 247.
- 7 W. van Schaik, S. Lizzo, W. Smit and G. Blasse, *J. Electrochem. Soc.*, 1993, **140**, 216.
- 8 C. Wickleder, *Z. Naturforsch.*, 2002, **57b**, 901.
- 9 L. Seijo and Z. Barandiarán, *J. Chem. Phys.*, 2014, **141**, 214706.
- 10 Z. Barandiarán and L. Seijo, *J. Chem. Phys.*, 2014, **141**, 234704.
- 11 E. Loh, *Phys. Rev.*, 1969, **184**, 348.
- 12 H. Witzke, D. S. McClure and B. Mitchell, in *Luminescence of Crystals, Molecules, and Solutions*, ed. F. E. Williams, Plenum, New York, 1973, p. 598.
- 13 S. B. Piepho, E. R. Krausz and P. N. Schatz, *J. Am. Chem. Soc.*, 1978, **100**, 2996.
- 14 R. A. Buchanan, K. A. Wickersheim, J. J. Pearson and G. F. Herrmann, *Phys. Rev.*, 1967, **159**, 245.
- 15 H. Przybylińska, C.-G. Ma, M. G. Brik, A. Kamińska, P. Sybilski, A. Wittlin, M. Berkowski, Y. Zorenko and V. Gorbenko, *et al.*, *Appl. Phys. Lett.*, 2013, **102**, 241112.
- 16 L. Seijo and Z. Barandiarán, *Phys. Chem. Chem. Phys.*, 2014, **16**, 3830.
- 17 V. Bachmann, C. Ronda and A. Meijerink, *Chem. Mater.*, 2009, **21**, 2077.
- 18 R. D. Shannon, *Acta Crystallogr., Sect. A: Cryst. Phys., Diffraction, Theor. Gen. Crystallogr.*, 1976, **32**, 751.
- 19 L. Seijo and Z. Barandiarán, *Int. J. Quantum Chem.*, 1996, **60**, 617.
- 20 A. Lupei, V. Enaki, V. Lupei, C. Presura and A. Petraru, *J. Alloys Compd.*, 1998, **275–277**, 196.
- 21 P. Yang, P. Deng and Z. Yin, *J. Lumin.*, 2002, **97**, 51.
- 22 C. W. Struck and W. H. Fonger, *J. Lumin.*, 1975, **10**, 1.
- 23 J. Gracia, L. Seijo, Z. Barandiarán, D. Curulla, H. Niemansverdriet and W. van Gennip, *J. Lumin.*, 2008, **128**, 1248.